Available online at www.sciencedirect.com
ScienceDirect
Cement and Concrete Research 37 (2007) 1115–1126
Cement and Concrete Research

Effect of steel microfibers on corrosion of steel reinforcing bars

J.A. Grubb [a], J. Blunt [a], C.P. Ostertag [a,*], T.M. Devine [b]

[a] Civil and Environmental Engineering Department, University of California, Berkeley, CA 94720, USA
[b] Materials Science and Engineering Department, University of California, Berkeley, CA 94720, USA

Received 10 November 2006; accepted 19 April 2007

Abstract

Steel microfiber reinforcement was previously found to be successful in mitigating alkali silica reaction in concrete, an expansive phenomenon. The use of steel microfibers to mitigate rebar corrosion, another expansive reaction, was investigated. Mortar specimens with and without steel microfiber reinforcement were exposed to a corrosive environment. All specimens were prepared with water/cement ratios of both 0.40 and 0.55, cured for 28 days, and then submerged in aerated 3.5% NaCl solution. The corrosion behavior of the specimens was monitored via electrochemical measurements. Three types of electrochemical tests were performed: corrosion potential measurements, potentiodynamic polarization, and electrochemical impedance spectroscopy. Chloride concentration measurements and microscopic analysis were performed as well. The polarization curves, Tafel, and polarization resistance measurements indicate that the steel rebar in the microfiber-reinforced mortars are more resistant to corrosion than the rebar in the control mortars, despite higher chloride concentrations. Furthermore, the steel microfiber-reinforced cement based materials have a lower electrolytic resistance. This is not indicative of a higher corrosion rate, which would be the case if it had been observed in standard mortar specimens.
© 2007 Elsevier Ltd. All rights reserved.

Keywords: Corrosion; Microfibers; Electrochemical measurements; Corrosion potential measurements; Electrochemical impedance spectroscopy; Tafel slopes; Polarization resistance measurements; Chloride concentration

1. Introduction

Steel microfibers were found to be successful in mitigating alkali silica reaction (ASR) [1–3]. Alkali silica reaction is a deteriorative mechanism that causes expansion and cracking in concrete. Cracks due to ASR start as microcracks in close vicinity to the reactive aggregate and hence microfibers were incorporated to control these microcracks at onset. Furthermore, microfibers are very effective in providing crack control through toughening mechanisms that promote crack growth resistance behavior [4,5]. Not only is the ASR gel formation delayed due to crack growth resistance behavior but also the ASR rate is considerably reduced [1].

It is hypothesized that corrosion, also an expansive process, can be mitigated with steel microfibers as well. When reinforcing steel within concrete corrodes, the rust product applies expansive pressure on the surrounding concrete inducing cracking in the matrix in close vicinity to the reinforcing steel. Corrosion then continues further and increased volume of rust product will propagate the microcrack and initiate others. When these cracks propagate far enough to reach the concrete surface, they become pathways allowing for the rapid ingress of water and chloride ions. Both agents accelerate the corrosion process, leading to further cracking and eventually to spalling.

Microfibers have an advantage over conventional macrofibers because they can influence the cracking process in close vicinity to the steel reinforcing bars at onset due to their small diameter. The microfibers will result in a higher required expansive pressure for cracks to initiate and propagate. Thus, for a constant corrosion rate, it will take longer for cracking to initiate in microfiber-reinforced specimens. Delaying crack formation will slow the corrosion process by preventing the corrosion products from leaving the reaction site.

In this study, steel microfiber-reinforced and plain mortar specimens with water/cement ratios of both 0.40 and 0.55 were exposed to sodium chloride solution and observed via electrochemical measurements over an extended period of

* Corresponding author.
E-mail address: ostertag@ce.berkeley.edu (C.P. Ostertag).

0008-8846/$ - see front matter © 2007 Elsevier Ltd. All rights reserved.
doi:10.1016/j.cemconres.2007.04.012

Table 1
Mix proportions

Batch designation	Mix proportions (relative weight ratios)				V_f (%)[a]	(Aggregate+fiber)/cement volume ratio
	Cement	Water	Sand	Fiber		
C40	1	0.40	1.82	0	0	2.15
F40	1	0.40	1.65	0.49	4.5	2.15
C55	1	0.55	2.82	0	0	3.33
F55	1	0.55	2.59	0.68	4.5	3.33

[a] Volume fiber/volume of mortar.

time. After 7 months, destructive tests were performed on half of the specimens. Electrochemical measurements, chloride content and microstructural analyses were performed and will be discussed. Three types of electrochemical tests were carried out: corrosion potential measurements, potentiodynamic polarization, and electrochemical impedance spectroscopy.

2. Experimental procedures and test setups

2.1. Specimen preparation

Four mortar mix designs were prepared and for each mix four specimens were cast in 75×150 mm cylinders. Of the four mortar mixes, two had a water cement ratio of 0.55 and two had a water cement ratio of 0.40. For each water cement ratio, one mix contained 4.5% (by volume) of steel microfibers while the other mix acted as a control with no fibers. The mix designs are given in Table 1. Superplasticizer was not used in this study to avoid any influence the superplasticizer might have on the corrosion reaction [6].

ASTM type I/II Portland cement was used for all mixes. The aggregate was Caltrans Sand with 1/8 in. maximum size aggregate and fineness modulus 3.12. The properties of the steel microfibers are given in Table 2.

Each 75×150 mm specimen contained a 9.52 mm nominal diameter reinforcing bar in its center. The rebar was cut into 180 mm lengths and at one end a flat spot was ground down on the bar's side. At the center of this flat spot a 3.6 mm diameter hole was drilled through the rebar. This hole was then threaded using an 8–32 tap. The rebar segments were then degreased with acetone, rinsed with methanol, and air dried. For this process, and until they were cast inside the mortar, the rebar segments were only handled with gloves to avoid the transfer of skin oils. Next, a ring terminal was attached to a short length of wire (approximately 75 mm) and placed on a small bolt. The bolt screwed into the previously drilled and tapped hole in the rebar (see Fig. 1). This provided a continuous electrical connection between the rebar and the wire that would protrude from the mortar. The bottom 1 cm of the rebar segment was coated with a commercially available micropore sealant, and allowed to air dry. The sealant was applied as extra insulation in addition to the heat shrink tubing applied next. The rebar segment was encased with heat shrink tubing so that only about 76 mm of the length of the rebar was exposed. Actual exposed length ranged from 74.5 mm to 76.8 mm, the exposed surface area was approximated as 22.7 cm^2. The rebar segments were placed within the mortar so that the exposed area was located at the center of the specimen.

Table 2
Steel microfiber properties

Cross section	(20–100 μm)×(100–140 μm)
Length (mm)	3–5
Elastic modulus (GPa)	200[a]
Tensile strength (GPa)	0.5–2.0[a]

[a] Typical values.

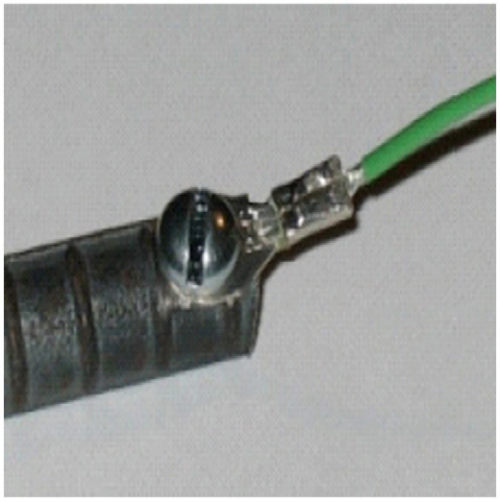

Fig. 1. Wire to rebar connection.

The specimens were cast in 75×150 mm cylinders in three lifts; the mortar was rodded and vibrated for each lift. The rebar was then placed into the mortar by holding the cylinder on the vibrator and slowly lowering the rebar into the mortar. Cardboard and binder clips were used to ensure the rebar was placed at the appropriate depth and as centered as possible. The specimens were placed in a fog room maintained at 25 °C and 100% humidity. After 24 h the specimens were demolded and returned to the fog room for a standard 28-day moist cure.

2.2. Electrochemical testing procedure

After curing for 28 days, initial electrochemical tests were performed on four of the specimens prior to exposing them all to chlorides. All of the specimens stood in approximately 38 mm of 3.5% sodium chloride (NaCl) solution for 24 h to promote absorption of the chlorides. All samples were then fully submerged in the NaCl solution. The solution was oxygenated via an air pump with three points of aeration (two at 750 cm^3 of air per minute, one at 1500 cm^3 of air per minute). The specimens remained submerged in this solution for the remainder of the study. Electrochemical tests were performed starting after 4 weeks and approximately every 2 weeks thereafter for the duration of the study. Three types of electrochemical tests were performed: corrosion potential measurements, potentiodynamic polarization, and electrochemical impedance spectroscopy.

2.2.1. Corrosion potential measurements

The measurement of the corrosion potential is covered in ASTM C-876 (Standard Test Method for Half-Cell Potentials of Uncoated Reinforcing Steel in Concrete) [7]. For this study a saturated calomel electrode (SCE) was used as a reference electrode. The tip of the reference electrode was placed on a wet sponge which was in direct contact with the surface of the specimen. The wet sponge provided continuous electrical connection between the SCE reference electrode and the specimen. With the voltmeter connected to the conventional reinforcing bar (working electrode) and the SCE reference electrode, the potential difference was measured. The corrosion potential, also called open circuit potential (E_{oc}), is a simple measure of the reinforcing steel's potential relative to the reference electrode.

It must be emphasized that the E_{oc} alone does not provide information on the corrosion rate of the specimen. In combination with a polarization curve (forward scan) or prior familiarity with the specimen, the E_{oc} may suggest a range of corrosion rates or indicate whether the specimen is actively corroding or passivated.

2.2.2. Potentiodynamic polarization tests

For a potentiodynamic polarization test the potential of the specimen is varied, forcing the specimen's potential away from its E_{oc}. When the specimen potential is not at E_{oc}, it creates an imbalance between the anodic and cathodic reactions that result in a net current. If no voltage is applied, the specimen potential remains at the open circuit potential and the current produced by the anodic and cathodic reactions are equivalent. In this case the net current is zero.

When a specimen is polarized to high degrees (on the order of 1V from E_{oc}), irreversible damage may occur that can modify future corrosion activity within the specimen [8]. For example, if a specimen originally in the passive range was polarized to a region of active corrosion, the specimen might not return to the initial passive state. If only one test is performed on the specimen, this is not of concern. But if, as in this study, many sequential tests are performed on the same specimen, the effect of the polarization must be accounted for. In this study, the range of polarization for each specimen was recorded and considered in the analysis of the data and determined to be of no effect for the polarization resistance measurements and the Tafel sweeps.

Potentiodynamic polarization tests were performed with a potentiostat and a three electrode setup. The three electrodes are the working electrode (in this case the steel rebar), the reference electrode (the same SCE used for the corrosion potential measurements), and a counter electrode. A stainless steel wire mesh was used as a counter electrode. By using a fine mesh (0.65 mm mesh spacing) counter electrode and wrapping it around the specimen, the resulting potential field was even and consistent around the exposed area of rebar. During these tests the specimens were submerged in NaCl solution up to the top 25 mm of the specimen. This provided full electrical contact between the counter electrode and the specimen. The top of the specimen was not submerged during electrochemical testing in order to prevent a direct electrical connection between the reference electrode and the counter electrode.

The primary purpose of potentiodynamic tests was to determine the corrosion current (I_{corr}). This is a measure of the rate of charge transfer between the anodic and cathodic reactions at the corrosion potential. The corrosion current density (i_{corr}), denoted by a lower case '*i*', is the I_{corr} normalized over the exposed area of steel in the working electrode. This assumes uniform corrosion is occurring across the entire surface of the bar. The corrosion current density cannot be directly measured, however the anodic/cathodic current differential can. Unfortunately this value is zero at the corrosion potential. Thus various analysis methods were utilized to estimate i_{corr}. These methods included Polarization Resistance, Tafel, and Cyclic Polarization. The same corrosion monitoring cell (described previously) was used for all tests. The difference was the range to which the specimen was polarized and how the data from the test was analyzed.

2.2.2.1. Tafel measurements. Tafel measurements provide data that can be used for more accurate estimates of I_{corr}. The data from this monitoring technique can be analyzed to determine the rate of current differential change as a function of the potential across the cell. These will be referred to as the Tafel slopes. For Tafel tests in this study, the specimens were polarized using a forward scan from $E_{oc}-50$ mV to $E_{oc}+50$ mV at a scan rate of 0.5 mV/s.

For most conditions of corrosion both the anodic and cathodic reactions are controlled by the kinetics of the electron transfer reaction at the metal surface, which is directly influenced by the magnitude of the potential field. The Butler–Volmer Eq. (2.1) models the charge differential between the anodic and cathodic reactions [9]:

$$I(E) = I_{corr} \cdot \left[e^{2.303 \cdot \frac{(E-E_{corr})}{\beta_a}} - e^{2.303 \cdot \frac{(E-E_{corr})}{\beta_c}} \right] \quad (2.1)$$

where:

$I(E)$	Net current differential between the anodic and cathodic reactions
E	Applied potential
I_{corr}	The corrosion current
E_{corr}	Potential where $I(E)=0$ (for unperturbed systems this is the corrosion potential, E_{oc})
β_a, β_c	Respective rates of the anodic and cathodic current change versus potential.

It must be emphasized that for large potential scans (E_{oc} +/− 100 mV), a best fit of the scan data to Eq. (2.1) will produce values of E_{corr} that are significantly different from the initial E_{oc}. In this case, the value of I_{corr} produced from the fit does not reflect the actual corrosion rate of the system. Methods that utilize a low potential scan magnitude must be used for accurate measurement. A non-linear best fit algorithm was developed for the Tafel data analysis that utilized genetic optimization in combination with an unconstrained non-linear optimization

(UNO). The objective function used was a normalized sum of the squares (2.2):

$$\Pi = \sum_i \left(\frac{I_{m_i} - I_{f_i}}{I_{m_i}} \right)^2 \quad (2.2)$$

where:

Π	Objective function value (error)
I_m	Array of measured currents (experimental data)
I_f	Array of best fit currents.

The genetic algorithm provided the initial values for the fit, which were then fed to the UNO, which found the local minimum. In this manner the values of the anodic and cathodic Tafel slopes were accurately determined. However, results from a Tafel analysis should be used with caution if the diffusion of oxygen or hydrogen ions is the rate limiting step. Alteration of the surface during the test (oxide formation for example), multiple simultaneous cathodic or anodic reactions, or a severe potential drop can also disrupt a Tafel analysis [9].

2.2.2.2. Polarization resistance. Polarization Resistance measurements require the specimen to be polarized a relatively small amount. For this study the specimens were polarized from $E_{oc}-10$ mV to $E_{oc}+10$ mV. ASTM G-59 (Standard Test Method for Conducting Potentiodynamic Polarization Resistance Measurements) [10] recommends a polarizing sweep from $E_{oc}-30$ mV to $E_{oc}+30$ mV, however the +/−10 mV sweep used for this study is an acceptable alternative. By only polarizing a small amount (close to E_{oc}) the plot is approximately linear thus the Butler–Volmer equation (see Eq. (2.1) above) can be simplified to the Stern–Geary Eq. (2.3) [9].

$$i_{corr} = \frac{B}{r_p} \quad (2.3)$$

where:

i_{corr}	Corrosion current density (units of current/area)
r_p	Polarization resistance of the steel ($r_p = \Delta E / \Delta i$ at $E = E_{oc}$)
B	The Stearn–Geary Constant

$$B = \frac{\beta_a \cdot \beta_c}{2.303 \cdot (\beta_a + \beta_c)}. \quad (2.4)$$

The polarization resistance, r_p, is the tangent of the $i(E)$ curve at E_{oc}, thus i_{corr} can be calculated once the value of B is known. The magnitude of B may be determined from a separate Tafel test, as was done in this study, or estimated based on familiarity of the specimen and its condition. A low scan rate of 0.125 mV/s was used for accurate current measurement. The ohmic drop was compensated during these experiments in order to provide accurate measurements of r_p independent of the difference in electrolytic resistance associated with inclusion of the metallic microfibers.

The primary disadvantage of the polarization resistance method is that the exact corrosion rate cannot be determined from this test alone. An accurate estimate or measure of the Stearn–Geary constant is required to calculate corrosion rate based on the magnitude of r_p. The advantages of using polarization resistance measurements are that it is a very quick measurement and it does not appreciably polarize the specimen.

2.2.2.3. Cyclic polarization curves. Cyclic polarizations consist of a large magnitude forward scan followed immediately by an equivalent reverse scan. For this study cyclic polarizations scanned from −1V to +1V and back to −1V. A moderate scan rate of 1.0 mV/s was used to reduce the test time without significantly reducing the accuracy of the current measurement. Although the data collected theoretically could be used for Tafel or polarization resistance calculations, the scan rate is generally too high for accurate measurements, and the large potential sweep can alter the corrosion rate even as the measurement is made.

2.2.3. Electrochemical impedance spectroscopy

Impedance is a more complex measurement than resistance. Resistance is the ability of a circuit to resist the flow of electrical current and is defined by Ohm's law: $R = E/I$. However, resistance only applies to the ideal resistor. The ideal resistor has limited applicability in real circuits because they are simplified in that they always follow Ohm's law, R is independent of frequency, and current and voltage signals are in phase [9]. Impedance is also a measure of the circuit's ability to resist current flow but it is not as limited as resistance. Impedance is defined as $Z = E/I$, where E and I are functions of frequency, time, and phase shift.

2.2.3.1. Impedance measurement. For electrochemical impedance spectroscopy (EIS), a small (1 to 10 mV) alternating (AC) potential is applied with a certain frequency and the AC current magnitude and phase shift are measured [8]. By keeping the excitation signal small, the response will be pseudo-linear which simplifies analysis. The frequency of the excitation is then changed and the current and phase shift re-measured. The range of frequencies applied is usually very large, and may include six orders of magnitude or more. For this study the frequency range was 10 mHz to 10 kHz. For EIS tests, the same three electrode setup was used as for all the potentiodynamic tests. Impedance analyses were carried out in order to determine the effect steel microfiber inclusion would have on the electrolytic resistance properties of the mortar composite.

2.3. Chloride content measurement

At 22 weeks of exposure time, half of the specimens were removed from the NaCl solution. Of the eight specimens, the four chosen specimens were F40B, F55D, C40D, and C55B. Each of these four specimens were cut into 6 slices on the order of 21.5 mm thick (see Fig. 2) and then oven dried at 110 °C overnight. Oven drying satisfied both preparation requirements for later tests and stopped corrosion by removing water from the mortar. The 1st and 6th slices were not used because chlorides penetrated from both the end and edge of the sample, resulting

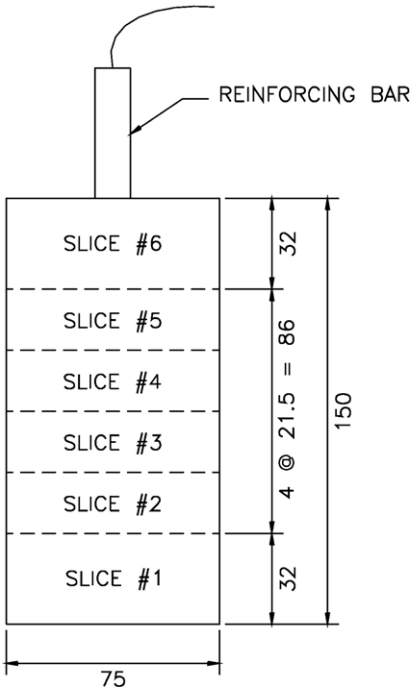

Fig. 2. Schematic of specimen cuts [mm].

in disproportionately high chloride content. Furthermore, the rebar segments contained in the 1st and 6th slices were covered by heat shrink tube.

One of the 4 viable slices of each specimen was used for chloride content analysis. The chosen slice for each specimen was then cut again as shown in Fig. 3. As measured from the outside diameter, the 0–13 mm sections were designated the 'Outer' sample; the 13–22 mm sections were designated the 'Inner' sample; and the 22–31 mm section was designated the 'Rebar' sample. The sections were ground dry with a vibratory micro-mill (ball mill) to pass through a #20 sieve. These samples were then sent to a commercial testing lab where an acid soluble chloride content analysis was performed (ASTM C-1152) [11].

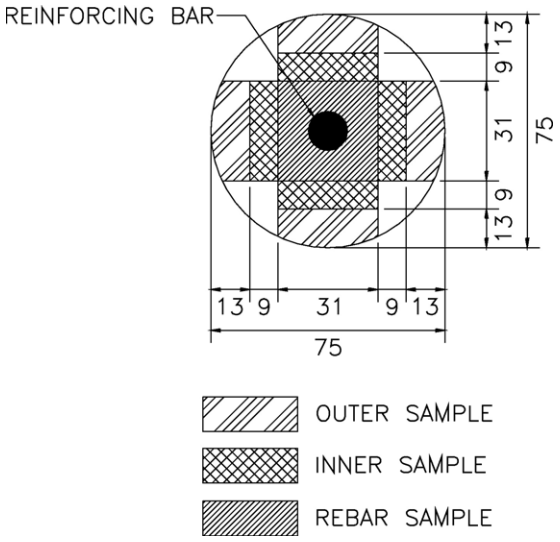

Fig. 3. Schematic of cuts for chloride content analysis [mm].

2.4. Microscopic analysis

The three viable slices for each specimen that were not used for chloride content analysis were epoxy coated immediately after removal from the oven. An epoxy was applied to the mortar slices under vacuum to avoid air bubbles and promote full penetration. The epoxy was then cured in air for three days. The epoxy filled all voids in the surface of the mortar slice up to a penetration depth of 1–2 mm into the mortar and effectively stopped corrosion. One epoxy coated slice was chosen for each specimen and cut to approximately 38 × 25 mm with the rebar in the center of the sample. These 4 samples were then ground and polished sequentially with 9 micron grit, 3 micron grit, 3 micron paste, and finished with 1/4 micron paste. The polishing removed the surface layer of epoxy, exposing the steel, aggregate, and cement paste, leaving only epoxy in the voids. This exposed the steel to corrosion processes, so from this point forward, the samples were stored in a vacuum desiccator when not in use to minimize the sample's contact with water. The samples were first examined under an optical microscope under regular light and also under blue fluorescent light. After the optical microscopy, the samples were prepared for scanning electron microscopy (SEM).

3. Results and discussion

3.1. Chloride content analysis

Fig. 4 and Table 3 display the chloride content at various depths within the specimens. Normalizing the Cl^- concentrations with respect to cement weight provides a meaningful measure because it is the $[Cl^-]/[OH^-]$ that control reinforcing steel depassivation. The concentration of chloride was similar at the exterior for all the specimens, with the exception of F55D. F55D had the highest chloride concentration at the exterior and at the depth of the rebar and its concentration at the rebar was higher than the exterior concentrations of the other three

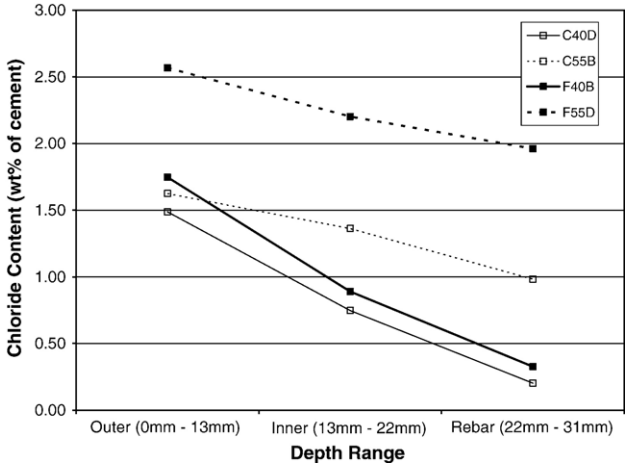

Fig. 4. Chloride content profiles.

Table 3
Chloride content profiles

Depth range	Chloride content[a]			
	C40D	C55B	F40B	F55D
Outer (0–13 mm)	1.49%	1.62%	1.75%	2.57%
Inner (13–22 mm)	0.75%	1.36%	0.89%	2.20%
Rebar (22–31 mm)	0.20%	0.98%	0.33%	1.96%

[a] Values expressed as a weight percent of chloride to cement.

specimens. This almost full penetration of Cl^- can be attributed to the expected high porosity of the specimen. C55B had the second highest concentration at the rebar depth with approximately half the Cl^- as F55D. F40B and C40D had similarly low concentrations, both approximately half of the concentration of C55B, although C40D was slightly lower. Because no superplasticizer was used, the fibers significantly decreased workability which led to a high occurrence of air voids and increased porosity and permeability. Air voids were also visible on the specimen surfaces.

For typical concrete mixes the critical chloride content for rebar corrosion is between 0.6 and 0.9 kg of Cl− per cubic meter of concrete [12]. If 400 kg/m^3 is assumed to be a nominal amount of cement in a typical concrete mix design, the critical chloride concentration may be stated in terms of weight percent of cement. This value is between 0.15% and 0.23%. The weight percent of chloride in all the samples was in excess of this range. However, this critical value is for concrete and is likely based upon water soluble chloride content, thus it is an underestimate for the critical acid soluble chloride content of mortar samples. Raupach and Dauberschmidt [13] reported that the critical chloride content to initiate corrosion of steel fibers is greater than 3.9% by weight of cement. Although not specified, it is likely that the reported critical chloride content is the water soluble content. They further found that the critical chloride content increases slowly with decrease in fiber diameter. Due to the fact that the smallest fiber they tested was 0.5 mm in diameter, and the fibers used in this study are 50 μm × 100 μm in cross section, the critical chloride content to depassivate the microfibers would be higher. It follows that the fibers are not at risk to corrosion because none of the samples had a chloride content exceeding 3.9%.

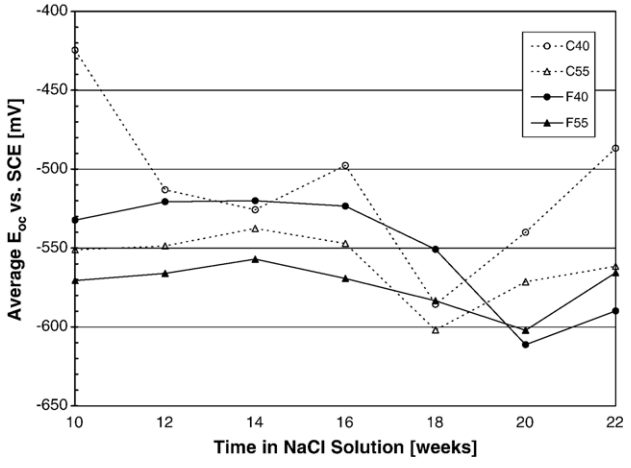

Fig. 5. Average corrosion potentials.

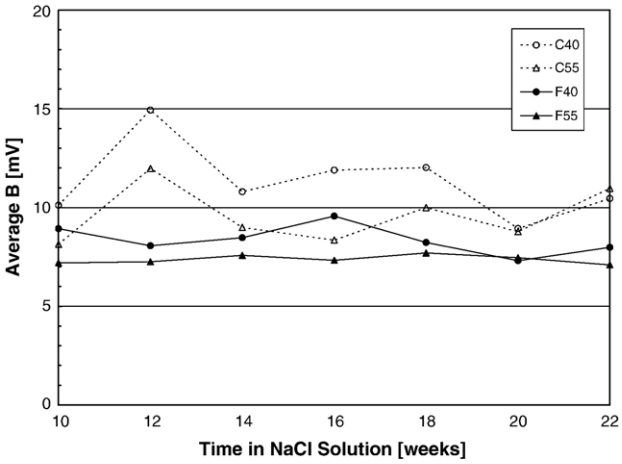

Fig. 6. Average Stearn–Geary constants.

3.2. Electrochemical tests

3.2.1. Corrosion potential measurements

Corrosion potentials were monitored and the results are shown in Fig. 5. The data for each mix is representative of the average value between two identical specimens tested. The period between 10 and 22 weeks was isolated because it was judged that a relatively steady-state condition had been reached during this time. Throughout this observation period, the potential values for the control specimens (without microfibers) appeared to be less negative than their microfiber-reinforced counterparts. At 22 weeks the average F40 corrosion potential was −589.9 mV while the value for C40 was −486.7 mV. This would be indicative of higher corrosion rates in the microfiber-reinforced specimens, however it will be demonstrated that this is in fact not the case and that E_{oc} cannot be relied on alone for accurate assessment of relative corrosion rates.

3.2.2. Tafel and polarization resistance

3.2.2.1. Tafel results. Fig. 6 provides a plot of the Stearn–Geary constant (B) as a function of time in the NaCl solution. According to Eq. (2.4), B is calculated from the anodic (β_a) and cathodic (β_c) Tafel slopes which are determined by the non-linear regression across the experimental Tafel data. Fig. 6 provides the average value calculated between the two specimens tested for each mix. Alone, the constant does not provide a means to calculate the corrosion rate; however a relative comparison provides insight to the effect of fiber addition. The general trend is for the microfiber specimens to exist at lower values of B when compared to their control counterparts. A comparison of average values results in the following. The average B value for the C40 specimens ranges between 8.9 and 14.9 whereas the value for the F40 specimens ranges between 7.3 and 9.6. A comparison between C55 and F55 results in the ranges 8.1 to 12.0 and 7.1 to 7.7 respectively.

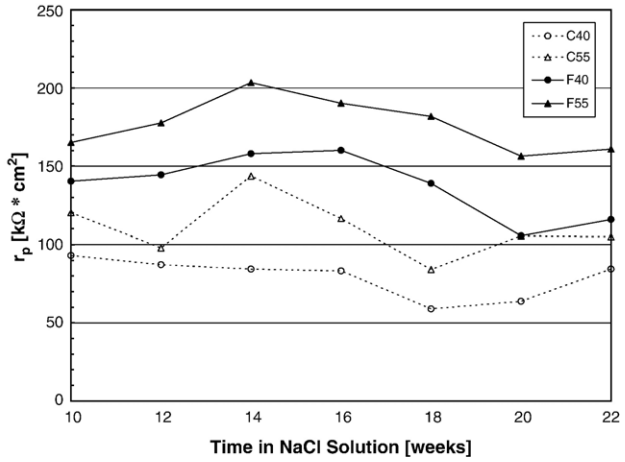

Fig. 7. Average polarization resistances.

3.2.2.2. Polarization resistance results. Fig. 7 provides a summary of the average polarization resistance values obtained from the tangent of the $i(E)$ curve at E_{oc}. microfiber-reinforced specimens show consistently higher r_p values (on the order of 50%) when compared to their control counterparts. Average values for the C40 specimens ranged between 58.9 and 93.1 kΩ cm^2 where the F40 specimens showed values on the order of 105.5 to 160.1 kΩ cm^2. A comparison between C55 and F55 showed ranges on the order of 84.1 to 143.6 kΩ cm^2 and 156.4 to 203.4 kΩ cm^2 respectively. This, in combination with the Stearn–Geary values determined from the Tafel sweeps provides strong evidence for reduced corrosion rates in the microfiber-reinforced specimens.

Fig. 8 shows the corrosion current density (i_{corr}) calculated by way of Eq. (2.3). The average value between the C40 specimens yielded the highest corrosion rates while the average between the F55 specimens yielded the lowest for the duration of the observation period. The difference in corrosion rates is distinct enough to assert that the inclusion of microfibers does reduce the corrosion rate of conventional steel reinforcing bars embedded in mortar. However the mechanism is not clear. A more detailed discussion of possible mechanisms and how they related to the microscopic evidence is discussed in Section 4. The corrosion current density of the C40 and F40 exceeds the corrosion current density of the C55 and F55 specimens. Microstructural analysis revealed that the C40 specimens exhibit considerably more microcracks around the steel reinforcing bar compared to C55 specimens. The difference in corrosion current density may be associated with the higher cement volume content in C40 and F40 specimens compared to the C55 and F55 specimens which may have induced thermal microcracking around the steel reinforcing bar.

3.2.3. Cyclic polarization curves

Fig. 9a plots the cyclic polarization curves for specimens C40D and F40B while Fig. 9b shows the cyclic polarization curves for C55B and F55D. All cyclic polarization measurements were made at 22 weeks with a forward scan range of −1.0 V to +1.0 V and a reverse scan range of +1.0 V to −1.0 V. Cyclic polarization measurements were made on specimens reserved for the destructive procedures such as chloride content analysis and microscopy. The w/c=0.40 specimens showed equivalent behavior in the passive regime for both the forward and reverse scans. Reduced corrosion rates during the reverse scan indicated that the increased oxidation rate in the transpassive region was not due to corrosion of the steel but instead due to oxygen evolution. Oxygen evolution is the oxidation of water as described in Eq. (3.1):

$$1/2\ O_2 + H_2O + 2e^- \rightarrow 2(OH^-) \quad (3.1)$$

Specimens with w/c=0.55 yielded equivalent passive behavior for the forward scan; however the reverse scan revealed dramatically different results. The measured current densities in F55D exceeded the forward scan passive values by an order of magnitude, instead of a reduction observed in all the other specimens. This is indicative of the fact that chloride contents were high enough for pitting corrosion to control over oxygen evolution at higher values of applied potential. The pitting potential for F55D is approximately +200 mV.

Observation of the average equilibrium potentials showed that the general tendency was for stabilization within the approximate range of −400 mV to −600 mV. During this period of stabilization, the least negative value was −425 mV while the most negative value was −611 mV. Thus, throughout the duration of the study, the corrosion state of the specimens existed at the border between the active and passive regions (Fig. 10). Consequently the pitting behavior, observed to occur above +200 mV had no relevance to the actual behavior of the undisturbed specimens. The only region of the polarization curves that is indicative of the actual behavior is the region of the equilibrium potentials. It is within this region that the control specimens had notably higher current densities, signifying the control specimens are more susceptible to corrosion than the microfiber-reinforced specimens.

Although not directly descriptive of the actual specimen behavior, the pitting corrosion at high applied voltages is suggestive of the chloride concentration. The chloride content analysis showed F55D to have the highest chloride content of the samples

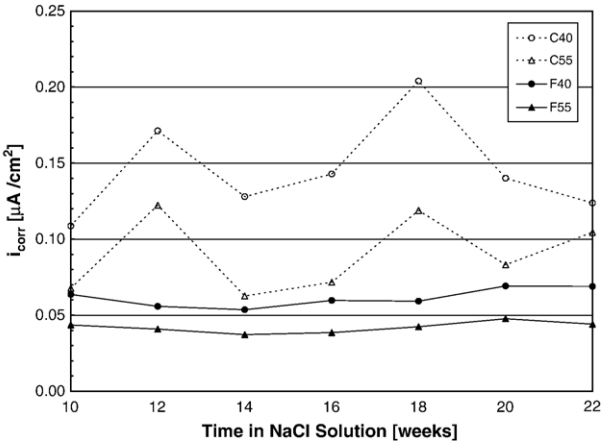

Fig. 8. Average corrosion current densities.

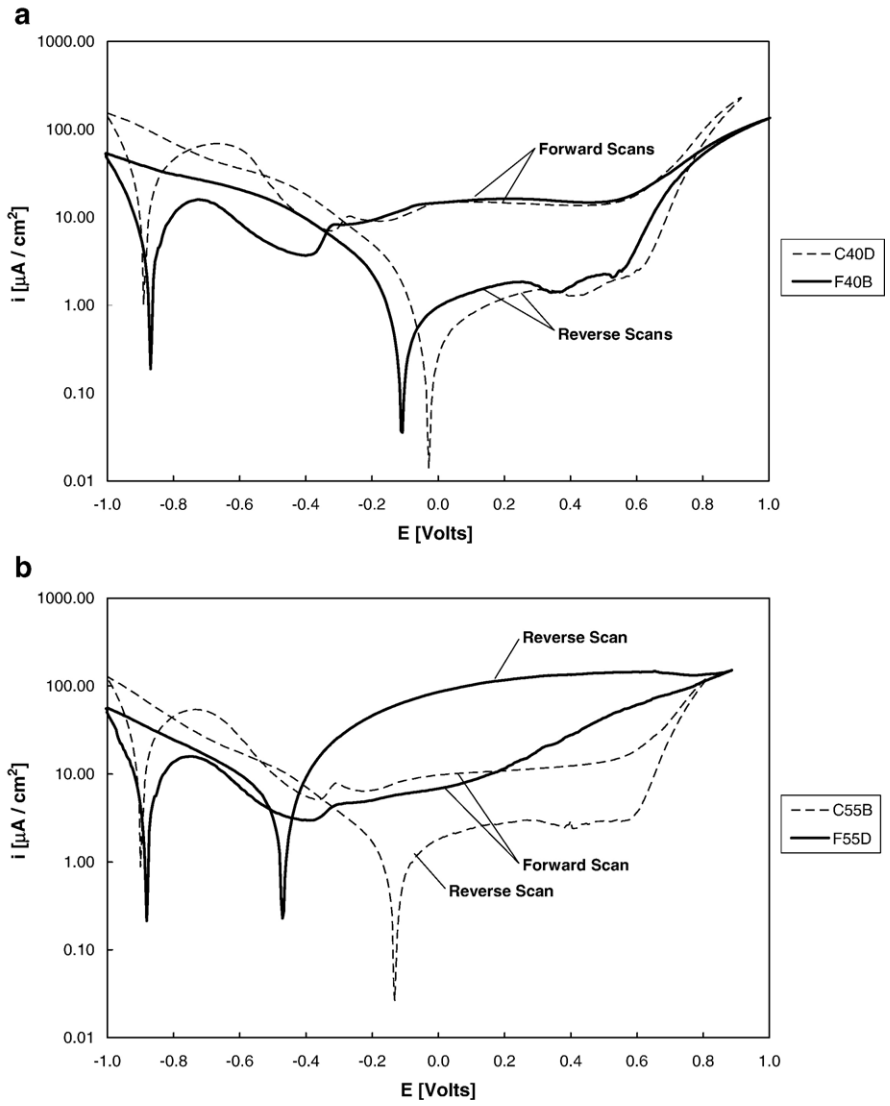

Fig. 9. a: Cyclic polarization scans for w/c=0.40 specimens (22 weeks). b: Cyclic polarization scans for w/c=0.55 specimens (22 weeks).

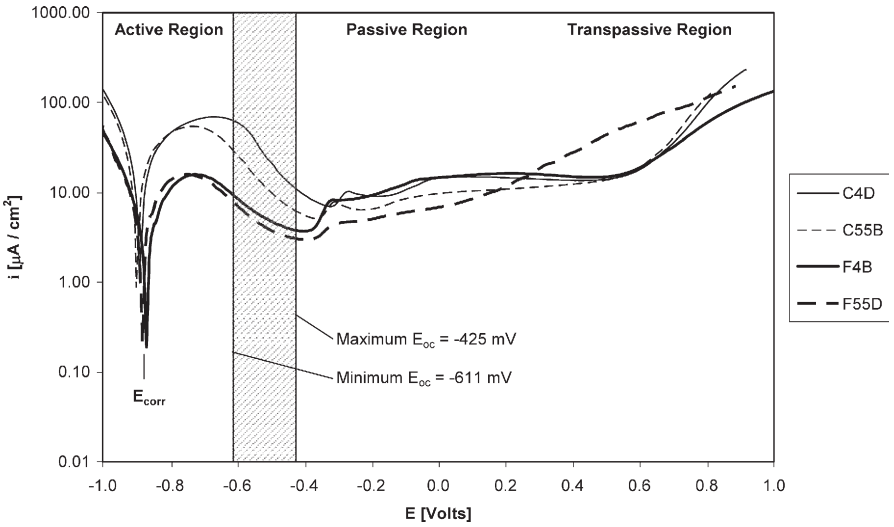

Fig. 10. Observed equilibrium potential range superimposed over 22 week forward polarization scans.

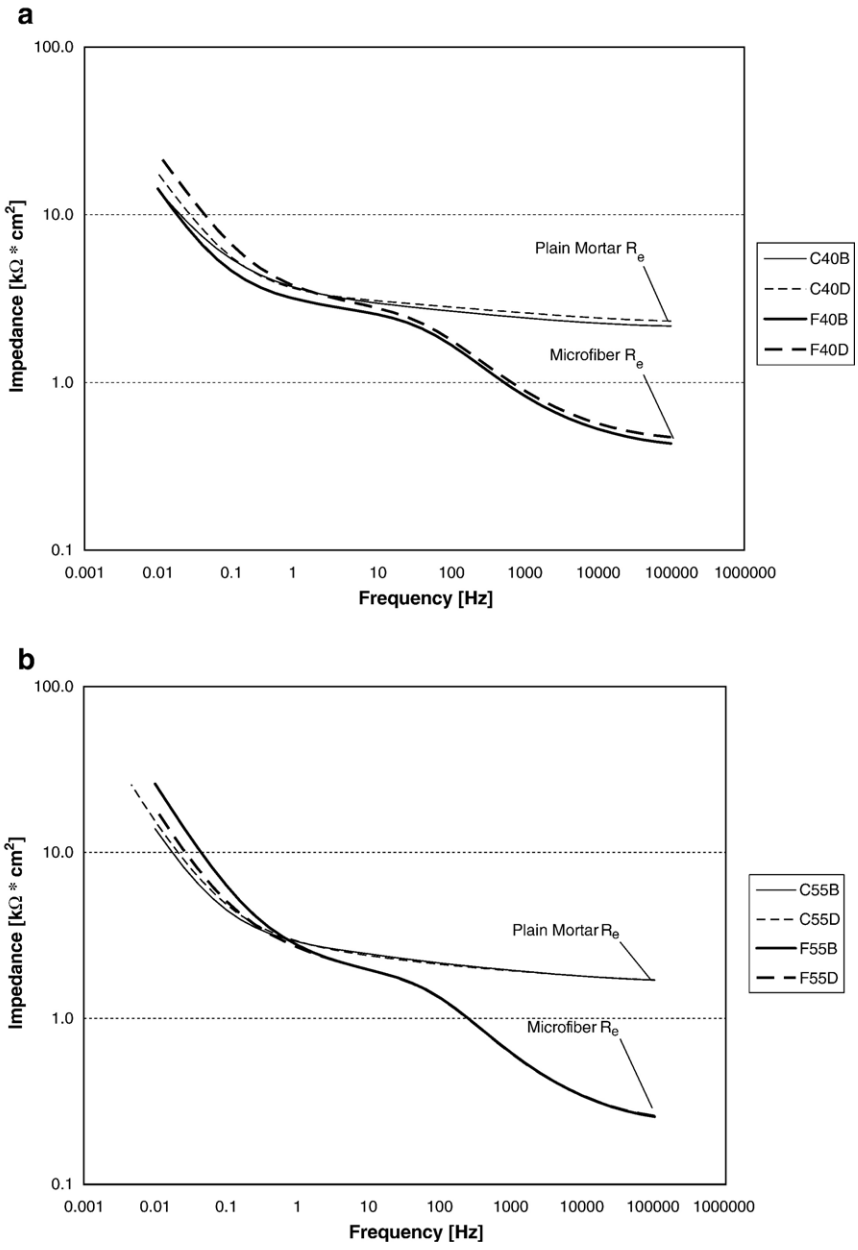

Fig. 11. a: Bode plot for w/c=0.40 specimens at 22 weeks of exposure. b: Bode plot for w/c=0.55 specimens at 22 weeks of exposure.

at the rebar surface (1.96%), while the chloride analysis showed C55B to have the second highest chloride content (0.98%). C40D and F40B were measured as having the lowest chloride contents (0.20% and 0.33% respectively); none of the 0.40 water–cement ratio specimens displayed pitting corrosion. Thus, the observed pitting corrosion behavior was due to the combination of applied high voltages and the chloride content; not the corrosion resistance behavior of the specimens in an unperturbed state.

3.2.4. Electrochemical impedance spectroscopy

Fig. 11a and b show the typical impedance plots (Bode plot) for all the mortar mixes. The higher frequency behavior (>mHz) was highlighted in order to accent the differences associated with the electrolytic resistance (R_e). From a conceptual point of view, this is the electrical resistance associated with ionic flow of the mortar matrix for the control specimens and the microfiber/mortar combination for the microfiber-reinforced specimens. The control specimens appeared to follow the typical curve associated with the Randles cell (single time constant). Although the test was not continued long enough to indicate the polarization resistance (R_p), the magnitude of R_e for the control mortars fell within the range of 1.7 to 2.3 kΩ cm^2.

The microfiber-reinforced specimens clearly differ from the control specimens and the typical Randles cell. In comparison to the curves for the control specimens it can be seen that the plateau in the curve in the range from 1 Hz to 100 Hz matches the value of R_e measured in the control specimen. At frequencies greater than 100 Hz the impedance continues to decrease, and stabilizes in the range of 0.26 to 0.47 kΩ cm^2 at a frequency of about 100 kHz. Due to this deviation between the

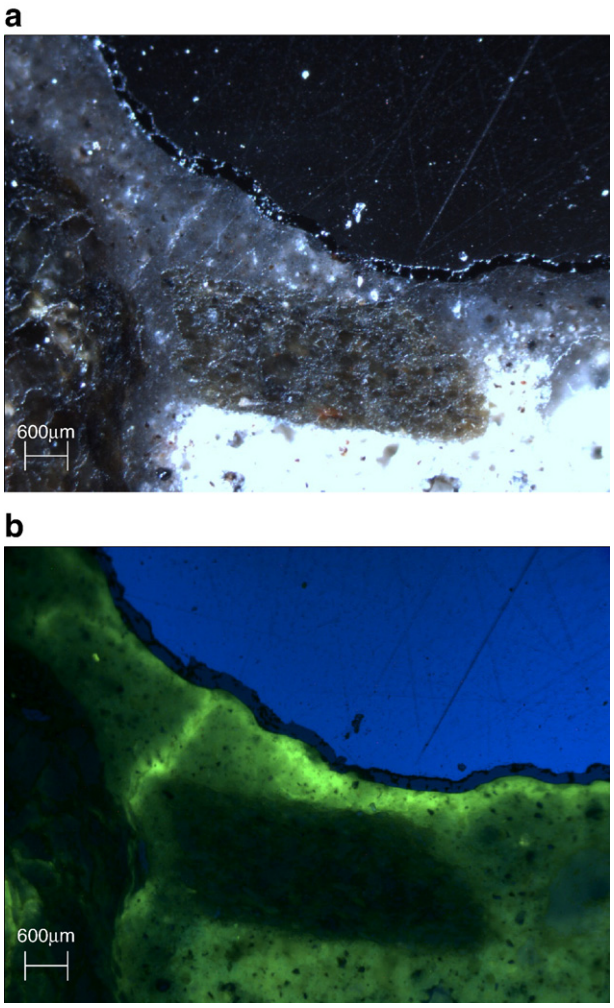

Fig. 12. a: C55B sample under normal light. b: C55B Sample under blue fluorescent light ((to see image in color visit www.sciencedirect.com/web-editions/journal/00088846).

microfiber and control specimens, it is clear that the steel microfibers affect the electrolytic resistance.

The steel microfibers provide shortcuts for the electrical current because they are conductive elements. In cement based materials that do not have steel microfiber reinforcement, the measured electric current travels between the counter electrode and the working electrode via ionic flow in the concrete pore solution. When steel microfibers are present, the current will travel via ionic flow between fibers and via electron transfer within the fibers. Flow of electrons within a metal has a practical resistance of zero, thus when the path of the electric current in cementitious matrix is interrupted by the conductive fibers, the total resistance is reduced.

The resistance of a concrete or mortar specimen is frequently taken as proportionate to the limitation of ionic flow — the higher the resistance, the more limited the ionic flow. If the limit on ionic flow is great enough, corrosion risk is considered negligible because ionic flow is required for the corrosion cell. Similarly, concrete materials with low resistivity are considered to have higher risk of corrosion. However, this should not be applied to concrete materials with steel fiber reinforcement because the fibers may reduce the measured resistivity without affecting the rate of ionic flow.

3.3. Microscopic analysis

The samples were examined under an optical microscope using a regular light and a blue fluorescent light. Under the blue fluorescent light, the mortar matrix fluoresced green, aggregates ranged from non-fluorescing to a yellow–green fluorescence, the epoxy fluoresced yellow, and the steel fluoresced blue. Because the cracks and voids were filled with epoxy, they were highlighted in yellow. Iron oxide, namely the mill scale on the rebar, fluoresced a slightly darker blue than the steel itself.

Radial cracks were observed in control specimen C55B, emanating from the rebar into the mortar as shown in Fig. 12 taken under regular (Fig. 12a) and blue fluorescent light (Fig. 12b). The cracks were far more visible under the fluorescent light. These cracks could either be shrinkage cracks due to the sample preparation procedure, which severely dried the sample, or the cracks could have been there before drying due to corrosion. Small spots of possible corrosion were seen as small red colored areas on the

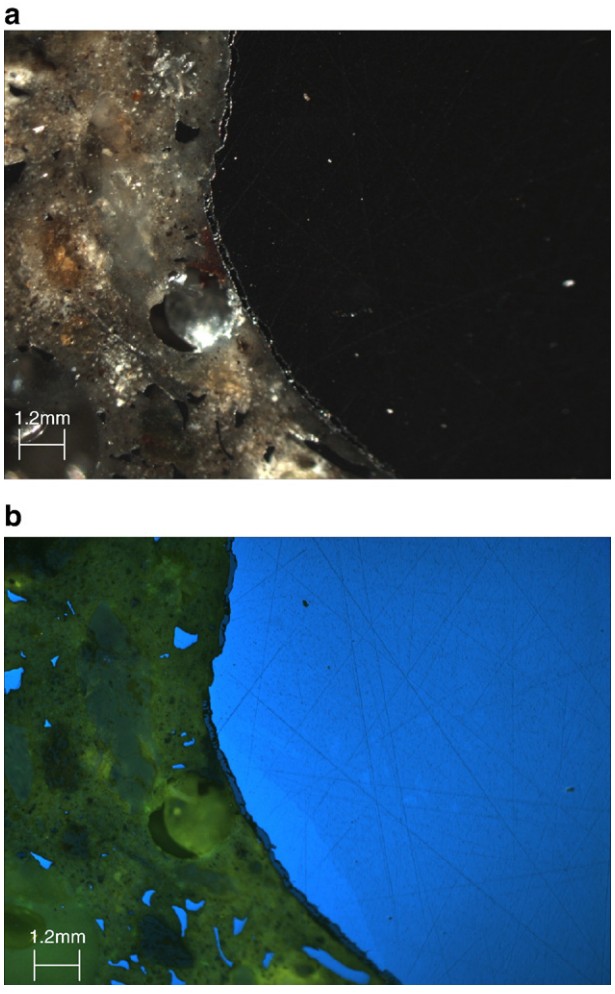

Fig. 13. a: F55D sample under normal light. b: F55D Sample under blue fluorescent light (to see image in color visit www.sciencedirect.com/web-editions/journal/00088846).

rebar–mortar interface under regular light. These spots were more visible when seen directly; the digital images were not very successful in capturing the colors. No cracks were observed in the microfiber-reinforced specimen F55D as shown in Fig. 13a and b, however, spots of possible corrosion were detected as well. Fig. 13 provided evidence that the microfibers were located in close vicinity to the steel rebar.

Under fluorescent light, the steel fluoresces blue. The region between the reinforcing bar and the matrix in Figs. 12 and 13, which fluoresced in a darker blue, was the mill scale on the rebar. Wherever corrosion spots were seen, they occurred where the mill scale was missing or cracked. None of the steel microfibers had mill scale, and none exhibited any possible rust spots, even near the exterior where the chloride content was highest. Mill scale, a surface layer of iron oxide that occurs as a normal result of hot rolling, cracks and fissures easily and is permeable to both air and moisture. Worse still, mill scale creates a galvanic couple with the underlying steel and promotes conditions for crevice corrosion of the reinforcing steel. Al-Zahrani [14] confirmed the mill scale's detrimental effect on corrosion behavior in a study that showed delayed initiation and reduced rate of corrosion for specimens without mill scale as compared to specimens with mill scale.

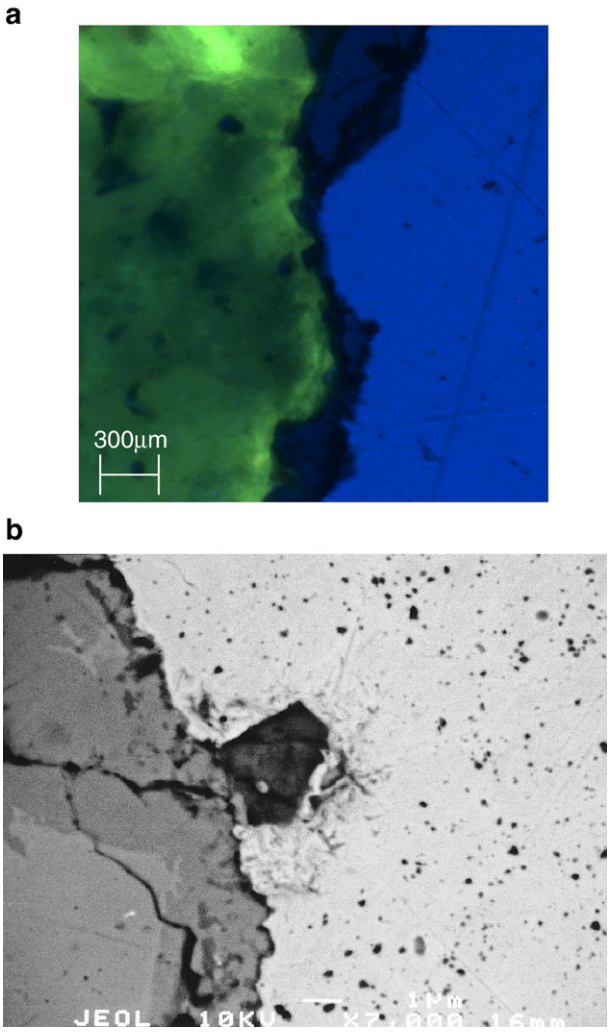

Fig. 14. a: C55B in Fluorescent Light ((to see image in color visit www.sciencedirect.com/web-editions/journal/00088846). b: Backscattered Electron Image at higher magnification.

Fig. 14 showed optical and SEM micrographs of the mill scale at various magnifications. The backscattered SEM image in Fig. 14b revealed cracks in the mill scale. Again, the mill scale was darker (similar in the optical micrographs) but here two shades were distinguished. This implied two different iron oxides in the mill scale, one with a higher percent of iron relative to oxide. Inside the magnified hole it was darker still. This may be yet another iron oxide, possibly a rust product. It may also be a void filled with epoxy, but this is unlikely as the void did not fluoresce like other epoxy filled voids when investigated under fluorescent light.

4. Discussion

The observed phenomena in this study were very peculiar due to the fact that their relationships seemed counterintuitive. It was observed that the highest Cl^- concentrations were found in the microfiber-reinforced specimens. This, coupled with the fact that a more negative corrosion potential and a lower electrolytic resistance were measured in the microfiber-reinforced specimens suggests that higher corrosion rates should occur in the presence of the steel fibers. However, this was not the case. Direct measurements of the polarization resistance and the Stearn–Geary constant yielded corrosion rates that were distinctly lower in the microfiber-reinforced specimens when compared to their control counterparts. In order to fully understand this phenomenon, the mechanisms of corrosion in a steel fiber reinforced matrix need to be isolated and examined in detail. The authors postulate that the fibers can influence both the cathodic and anodic reactions in a corrosion cell.

From the standpoint of the cathodic reaction, the addition of steel microfibers is immediate. The cathodic reaction can be controlled by the concentration of oxygen (Eq. (3.1)), so reductions in O_2 concentrations reduce the amount of available oxygen to carry out this reaction. Studies have demonstrated that steel fibers show increased corrosion resistance when compared to conventional steel reinforcement [13,15,16]. Coupled with the fact that corrosion was not observed on any of the fibers in this study, it is most likely that the fibers were in a passive state. Trejo [17] stated that the formation of the passive layer for steel in a cement based matrix is an oxygen intensive process. Whether by formation of stable oxides or direct adsorption of the oxygen to the surface of the steel, the addition of steel microfibers provide an extensive amount of surface area that can act as localized sinks and draw oxygen away from the steel reinforcing bar. For purposes of example, if the steel fibers are assumed to be prismatic in shape with nominal dimensions of $0.06 \times 0.12 \times 4$ mm, a 4.5% dosage of fibers by volume to a 75×150 mm cylinder would add over 15,500 cm^2 of added steel surface area. This is a significant amount considering the exposed area of conventional reinforcing bar steel used in this study was 22.7 cm^2. It is also anticipated that an environment devoid of available oxygen may modify the species of iron oxides that typically form in the wake of iron oxidation. Iron

oxide species with lower oxygen content have a lower molecular volume and hence are less expansive. In terms of cracking due to corrosion, expansive stresses due to the formation of corrosion products will be reduced in oxygen deprived environments. Confirmation of this theory must be verified in-situ because destructive techniques used to gain access to the cement/steel interface can drastically modify the state of oxidation.

In terms of anodic control, the fibers may act in much the same way they did in the presence of ASR. After sufficient concentrations of Cl^- are present or a carbonation front has reached the surface of the steel bar, corrosion can propagate unimpeded. In the case of conventional plain concrete, the formation of iron oxides induces expansive stresses which cause microcracking. Once a crack has formed, the magnitude of expansive stress required to propagate the crack are reduced [1,3] and the rate of ingress of deleterious compounds and the rate of egress of corrosion products is increased due to the crack opening. Microfibers close to the steel surface provide a source of passive confinement. Cracks can only propagate under increases in the magnitude of expansive stress [1]. In this way, expansive corrosion products that form near the surface of the steel bar remain there and collect. It is postulated that under this confined condition, the solid products formed from the corrosion process will fill surrounding voids and any cracks that may have initiated, locally densifying the cement matrix and cutting off the further ingress of deleterious compounds.

5. Conclusion

In this study, mortar specimens with and without steel microfiber reinforcement were exposed to a corrosive environment. Reinforced and control specimens were prepared with water/cement ratios of both 0.40 and 0.55, cured for 28 days, and then submerged in aerated 3.5% NaCl solution. The specimens remained continually moist, thus preventing any drying cracks. Electrochemical measurements were performed immediately prior to the immersion of the specimens, at 4 weeks of exposure, and at approximately 2-week intervals thereafter up to 7 months. Three types of electrochemical tests were performed: corrosion potential, potentiodynamic polarization, and electrochemical impedance spectroscopy. After 7 months, half of the specimens were tested for chloride content and examined under both optical and scanning electron microscopes. From this study, the following conclusions can be made:

1. Steel microfiber-reinforced cement based materials will have lower measured electrolytic resistance values, but unlike for standard mortars, this is not indicative of a higher corrosion rate.
2. Corrosion current density measurements based on polarization resistance and Tafel slope measurements indicate that the steel microfiber-reinforced mortars are more resistant to corrosion than the control mortars, despite higher chloride concentrations.
3. The mechanisms that caused reduced corrosion rates in the microfiber-reinforced specimens are not yet clearly identified and require further study consisting of precise experimentation designed to isolate the effect of each potential mechanism.

References

[1] C.K. Yi, C.P. Ostertag, Mechanical approach in mitigating alkali-silica reaction, Cement and Concrete Research 35 (2005) 67–75.
[2] F. Bekas, L. Turanli, C.P. Ostertag, New approach in mitigating damage caused by alkali-silica reaction, Journal of Materials Science 41 (2006) 5760–5763.
[3] C.P. Ostertag, C.K. Yi, P.J.M. Monteiro, "Effect of Confinement on the Properties and Characteristics of the Alkali-Silica Reaction Gel", ACI Materials Journal 104 (3) (2007) 303–309.
[4] C.K. Yi, C.P. Ostertag, Strengthening and toughening mechanisms in microfiber reinforced cementitious composites, Journal of Materials Science 36 (2001) 1513–1522.
[5] C.P. Ostertag, C.K. Yi, Crack/Fiber Interaction and Crack Growth Resistance Behavior in Microfiber Reinforced Mortar Specimens, Materials and Structures (in press) doi:10.1617/s11527-006-9181-1.
[6] T. Mohammed, H. Hamada, Durability of concrete made with different water-reducing chemical admixtures in tidal environment, ACI Materials Journal 100 (2003) 194–202.
[7] ASTM C-876-91, Standard test method for half-cell potentials of uncoated reinforcing steel in concrete, Annual Book of ASTM Standards, vol. 3.02, American Society for Testing and Materials, 1999.
[8] A. Bentur, S. Diamond, N.S. Berke, Steel Corrosion in Concrete: Fundamentals and Civil Engineering Practice, E&FN Spon, New York, 1997.
[9] Gamry Echem Analyst, Version 1.30. CD-ROM, Gamry Instruments, Inc., Warminster, Pennsylvania, 2003.
[10] ASTM G59-97, Standard test method for conducting potentiodynamic polarization resistance measurements, Annual Book of ASTM Standards, vol. 3.02, American Society for Testing and Materials, 2003, pp. 229–232.
[11] ASTM/C1152M-04, Standard Test Method for Acid-Soluble Chloride in Mortar and Concrete, In: Annual Book of ASTM Standards, v. 4.02, American Society for Testing and Materials, 1999, pp. 632–635.
[12] P.K. Mehta, P.J.M. Monteiro, Concrete: Microstructure, Properties, and Materials, 3rd ed.McGraw-Hill, 2006.
[13] M. Raupach, C. Dauberschmidt, Critical chloride content for the corrosion of steel fibers in artificial concrete pore solutions, in: V.M. Malhotra (Ed.), Proceedings of the Sixth CANMET/ACI International Conference on Durability of Concrete, American Concrete Institute, Farmington Hills, Michigan, 2003, pp. 165–180.
[14] M.M. Al-Zahrani, Effect of steel manufacturing process and atmospheric corrosion on the corrosion-resistance of steel bars in concrete, Cement and Concrete Composites 24 (2002) 151–158.
[15] P.S. Mangat, K. Gurusamy, Corrosion resistance of steel fibers in concrete under marine exposure, Cement and Concrete Research 18 (1988) 44–54.
[16] D.C. Morse, G.R. Williamson, Corrosion Behavior of Steel Fibrous Concrete, Construction Engineering Research Laboratory Technical Report CERL-TR-M-217, 1997.
[17] D. Trejo, Microstructural Design and Electrochemical Evaluation of Fe/2Si/0.1C Dual-Phase Ferritic Martensitic Steel for Concrete Reinforcement, Ph.D. Dissertation (1997).